
Article:
Yenne, E.Y. orcid.org/0000-0002-9647-5320, Green, C. orcid.org/0000-0001-9644-4949 and Torvela, T. (2025) Modelling geologic features and structures in the Middle and Lower Benue Trough of Nigeria from gravity and aeromagnetic data sets. Journal of African Earth Sciences, 231. 105745. ISSN 1464-343X

https://doi.org/10.1016/j.jafrearsci.2025.105745

Modelling geologic features and structures in the Middle and the Lower Benue Trough of Nigeria from gravity and aeromagnetic data sets

Yenne E.Y[*1], Green C.* and Torvela T.*
*School of Earth and Environment, Institute of Applied Geosciences, University of Leeds, Leeds, UK
Corresponding Author: ezekielyenne@gmail.com, **ORCID:** 0000-0002-9647-5320

Abstract:

Understanding subsurface structures is key to predicting the evolution of a basin and its resources. The Benue Trough is a mega-structure that has been moderately well studied, although a detailed regional subsurface study of the basin is lacking. Our aim in this study is to highlight and show clearly the subsurface geologic structures/features through 2D and 3D models. We used gravity and high-resolution aeromagnetic datasets to map and investigate geologic features and subsurface structural texture of the trough in 2 and 3 dimensions. We constructed geologic models in 2D from gravity and magnetic datasets and mapped basement faults, depth to basement, Curie, and Moho depths, and interpreted the crustal structure of the basin. Three well-defined basement fault systems were identified: NE-SW, NW-SE, and ENE-WSW. Based on basement fault kinematics through paleo-stress field interpretation, we showed that the basement faults evolved through plate tectonic activities at the earlier stage of the evolution of the trough. We then carefully modelled in 3D critical interfaces (basement surface, Curie isotherm, and Moho), where we estimated their depths and interpreted their morphologies. The average basement depth is 4.3 km and areas of basement lows are interpreted as sub-basins; these are suitable sites for the accumulation of sediments (depocentres) while the basement highs are considered basement uplifts and blocks. The Curie depth (the depth to the bottom of the magnetic layer) is relatively flat across the area while the Moho is uplifted directly under the basin. We observed the crust to be thinned directly under the basin which we attributed to extensional rifting processes. This study exposed the subsurface tectonic architecture of the trough and demonstrated its continental origin due to crustal rifting and extension, accompanied by faulting, Moho shallowing, magma emplacement, and crustal thinning and stretching.

Keywords: Aeromagnetic, gravity, modelling, basement depth, fault, Curie depth, Moho, crust.

Introduction

The Benue Trough is a rifted linear depression filled with about 6 km to 7 km of Cretaceous rocks bordered on the east and west by crystalline basement rocks (Fitton, 1980; Ajayi and Ajakaiye, 1986; Obaje, 2009). It spans from the Niger Delta in the South to the Bornu-Chad basin in the North measuring about 120 km and 800 km in width and length, respectively. The Benue Trough is oriented in a general Northeast-Southwest direction formed through several phases of tectonic activity (Ofoegbu, 1985; Fairhead and Okereke, 1987; Fairhead and Green, 1989; Akande *et al.*, 2012). The trough has been geographically divided into the Lower, Middle, and Upper parts based on stratigraphy; this study is focused on the Lower and Middle part (Akande *et al.*, 2012; Anudu *et al.,* 2014; Lar, 2015; Fig. 1). The subsurface structural architecture of the Lower and the Middle Benue Trough are yet to be fully understood. The geologic features/structures are in most cases deeply buried and very difficult to accurately map since they are covered with thick sediments, vegetation, and/or heavily weathered materials. Many scientists have faced the challenge of accurately mapping the subsurface structures and its morphology (Nwogwugwu *et al.*, 2017; Nwosu, 2014; Okiwelu *et al.*, 2014, Anudu *et al.*, 2020). This study, however, employed a more robust and integrated approach by applying the aeromagnetic and gravity datasets to model in 2D and 3D the morphology of the subsurface features such as the basement, Curie isotherm, and Moho depths.

2. The geologic and structural settings of the area

The geological setting of the area is generally composed of an underlying Precambrian Basement Complex and overlying Cretaceous sedimentary rocks with intra-sedimentary intrusive rocks (Benkhelil, 1989; Obaje, 2009; Akande et al., 2012; Fig. 2). The Precambrian Basement Complex is composed of a less metamorphosed series made up of gneisses, schists, and quartzites, and a highly metamorphosed series of banded and contorted gneisses (Cratchley and Jones, 1965; Ofoegbu, 1985). In each series are many major and minor intrusive rocks separated into younger and older intrusive rock types (Wright, 1968). The Cretaceous sedimentary rocks form a major part of the study area and overlie the Precambrian basement. The intrusive rocks were emplaced within the trough from Mesozoic to Cenozoic times in the form of sills, dykes, bosses, plugs, etc., and are found within or across folded and unfolded sedimentary rocks (Ofoegbu, 1985; Coulon et al., 1996; Anudu et al., 2014).

The Trough trends in a NE-SW direction with several tectonic features like sub-basins, uplifts, ridges, volcanic rocks, etc (Olade, 1975; Agagu and Adighije, 1983; Ofoegbu, 1985; Fairhead *et al.*, 2013). Evidence of faulting and compressional folding in general NE-SW, N-S, NW-SE, and ENE-WSW directions have been observed (Cratchley and Jones, 1965; Agagu and Adighije, 1983; Ofoegbu, 1985; Anudu *et al.,* 2014). Folding, faulting, and upliftment of the basement leading to the formation of structural features such as the Abakaliki anticline, the Anambra Basin, Afikpo synclines, the Keana anticline, and Awe syncline, etc., occurred during the Santonian tectonism (Agagu and Adighije, 1983; Akande et *al.*, 2012). The Post-Santonian sediments are not affected by these Santonian tectonic activities (Cratchley and Jones, 1965; Ofoegbu, 1985; Obaje, 2009; Fatoye and Gideon, 2013). The evolution of the area occurred alongside other large intercontinental basins in West Africa during the trans-tensional

regime of the Equatorial Atlantic between the Aptian and Albian times (Benkhelil, 1989). Many authors believed that these happened through a series of repeated tectonic activities leading to the present architecture (Fairhead and Okereke, 1987; Fairhead, 1992; Fairhead *et al.*, 2013; Abubakar, 2014).

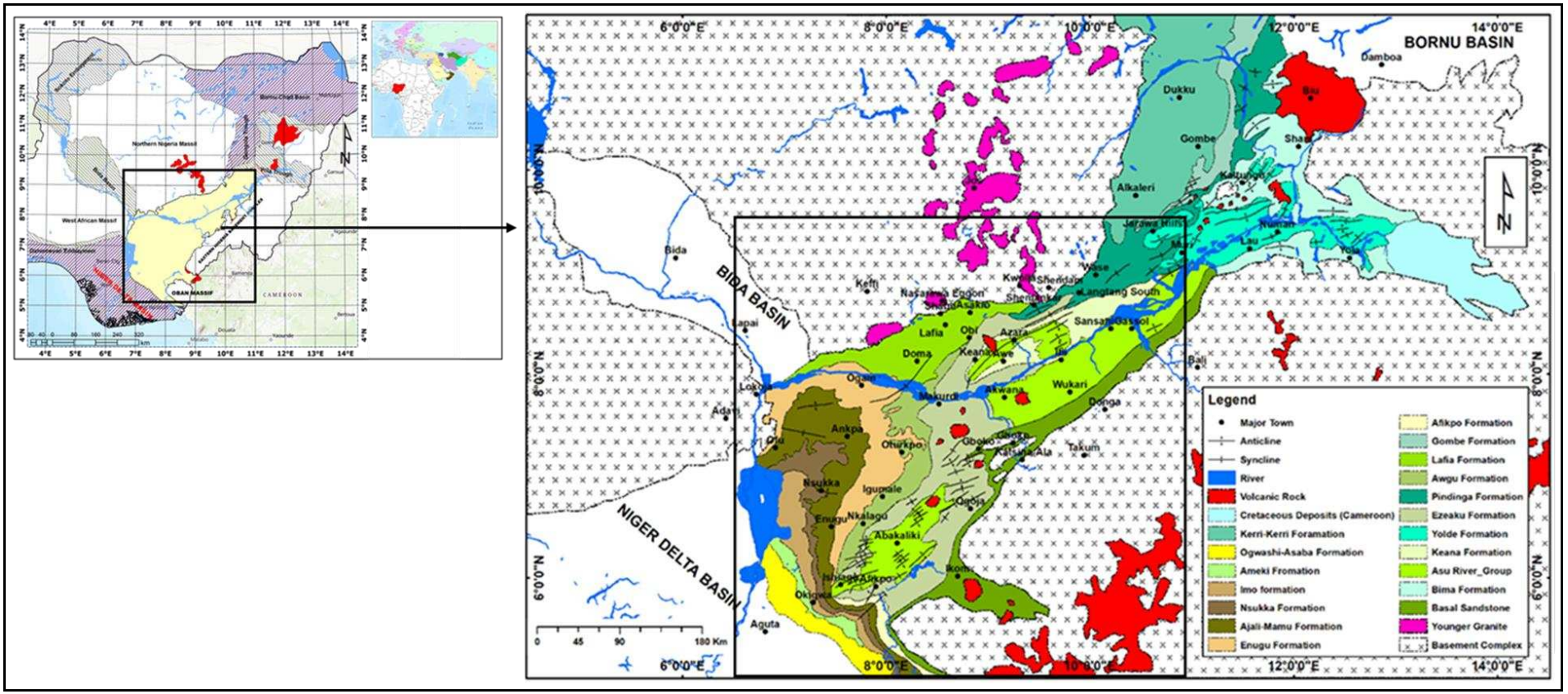

Fig. 1: Location and generalized geology of the Benue Trough with a simplified stratigraphic succession. The Upper Benue Trough is bordered to the NE by the Bornu Basin while the Lower Benue Trough is bordered to the SW by the Niger Delta Basin (modified after Guiraud and Maurin, 1992; Najime, 2011).

3 Data Processing

3.1 Gravity data

The gravity dataset used is compiled from land gravity point values and the Earth Gravitational Model 2008 (EGM2008, Pavlis et al., 2012). Land gravity was obtained using a reduction density of 2.67 g/cc with between +/- 0.5 mGal accuracy and +/-1 mGal error margin during measurement while the height accuracy ranges between 1.5 – 3 m. EGM2008 was created by integration of terrestrial, airborne, and satellite derived gravity. To this, we added ground gravity observations from various sources (Cratchley and Jones, 1965; Hospers, 1965; Cratchley et al.,1984; Okereke, 1984; Bomfim et al., 2013. Fig. 2 a). We interpolated and regridded the raw data at a cell size of 5 km by 5 km using the continuous curvature splines in tension in Oasis Montaj and smoothed with a 3 x 3 Hanning filter (Fig. 2 b). This filter was chosen because of its ability to blend and smoothen the appearance of the different data sets (land gravity data and the EGM2008 models) with varied resolutions. The Bouguer gravity anomaly grids has an average of 2.5 arc-minute by 2.5 arc-minute resolution. It is composed of a broad positive anomaly due to thinning of the crust beneath the basin (Fairhead and Green, 1989; Obasi et al., 2018). The positive anomalies at the centre have been attributed to shallow granitic basement and/or igneous intrusion and the uplift of the Moho and the negative anomalies to thick deposits of sediments (Ajayi, 1979; Adighije, 1981; Ajayi and Ajakaiye, 1981). The highest and lowest positive values are 102 mGal and -87.6 mGal, which are attributed to volcanic emplacement and sedimentary infills of the basins, respectively. Furthermore, the short and long wavelength variations in the Bouguer anomaly map indicate density variation from sediments, crust, and upper mantle (Welford & Hall, 2007; Dressel et al., 2018).

3.2 Magnetic data

The magnetic dataset used in this study is the high-resolution aeromagnetic grid provided by Fugro Airborne Surveys, surveyed at 500 m line spacing and 5000 m tie-line spacing between 2005 and 2007 for Nigeria. The datasets were recorded at 0.1 second interval with 80 m mean terrain clearance making the resolution better than earlier high-altitude data (Reford *et al.*, 2010; Anudu *et al.,* 2014). A bi-directional gridding technique (Geosoft, 2004; Foss, 2011) was used to produce a total magnetic intensity (TMI) grid at 125 x 125 m cell size and a map (Fig. 3 a). The TMI map shows magnetic values that range between -2330.6 nT and 1259.2 nT. They are characterized by anomalies that have short, medium, and long wavelengths. The short wave length (high wavenumber) anomalies are observed mostly outside the basin and in a few places within the basin typified by basement inliers and intrusive rocks. The long wavelength (low wavenumber) anomalies are seen within the basin signifying deep magnetic sources associated with the deep basement. The description of the characteristics and textures of the TMI map is a key component in interpreting magnetic signatures at or around the equator (Beard, 2000; Li, 2008); the range of magnetic field inclination in this area is from -16.43° to -4.37°.

We applied a reduction to the pole (RTP) transformation to the TMI map to vertically place anomalies over sources of disturbance (Swain, 2000; Li, 2008). However, the result shows extreme elongation of anomalies in the N-S direction due to the instability in the transform making the map uninterpretable (Tulyatid and Fairhead, 1996; Beard, 2000). The Differential

Reduction to the Pole (DRTP) technique was applied instead (Arkani-Hamed, 1988; MacLeod et al., 1993; Arkani-Hamed, 2007; Li, 2008). In this technique, the TMI map of the area was divided into eight (8) E-W strips with 1° latitude range and 30' overlap. The mean inclination and declination of each strip were estimated from the IGRF model, and the standard RTP using a pseudo-inclination of 30° to suppress noise was applied. Li, (2008) suggested that the best pseudo-inclination value is between 20° and 30°. We tested the values and observed a 30° pseudo-inclination gives the best result as it controls the amplification and to some extent filter out the N-S distorted magnetic anomalies. The strips were merged and filtered using a 3X3 Hanning filter to smooth and remove aliasing from the grid (Fig. 3 b). We mentioned the grid cell size as the same as the original data. This filter was chosen due to its suitability in smoothening any noise and distortion resulting from the DRTP transformation technique. This filter modified the magnetic anomaly as though it is at the pole with positive anomalies lying directly over the causative bodies with positive susceptibility contrast (Swain, 2000; Cooper and Cowan, 2005; Ali et al., 2017). The result shows that DRTP has successfully corrected for the blown-up N-S structures and highlights many of the magnetic sources. However, amplitudes have been significantly impacted by increasing its value during the process (e.g., the positive anomaly has increased from 1259 nT to 2008 nT and the minimum from -2330 nT to -2187 nT).

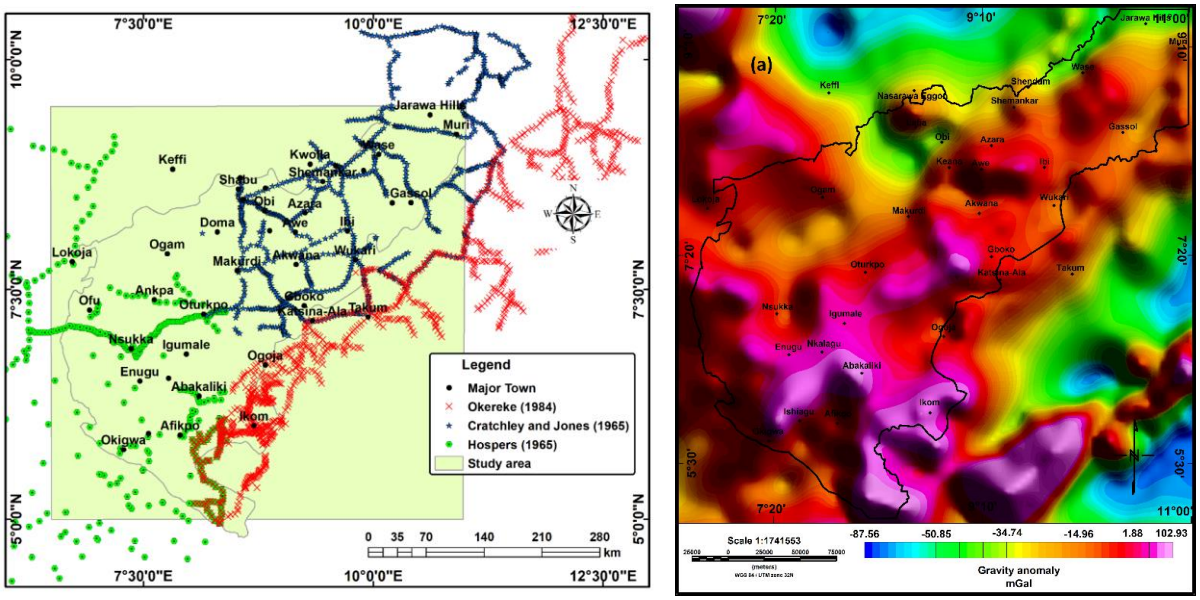

Fig. 2: (a) Land point data contributions (b) Shaded Bouguer anomaly map of the study area (Land point and EGM2008 data).

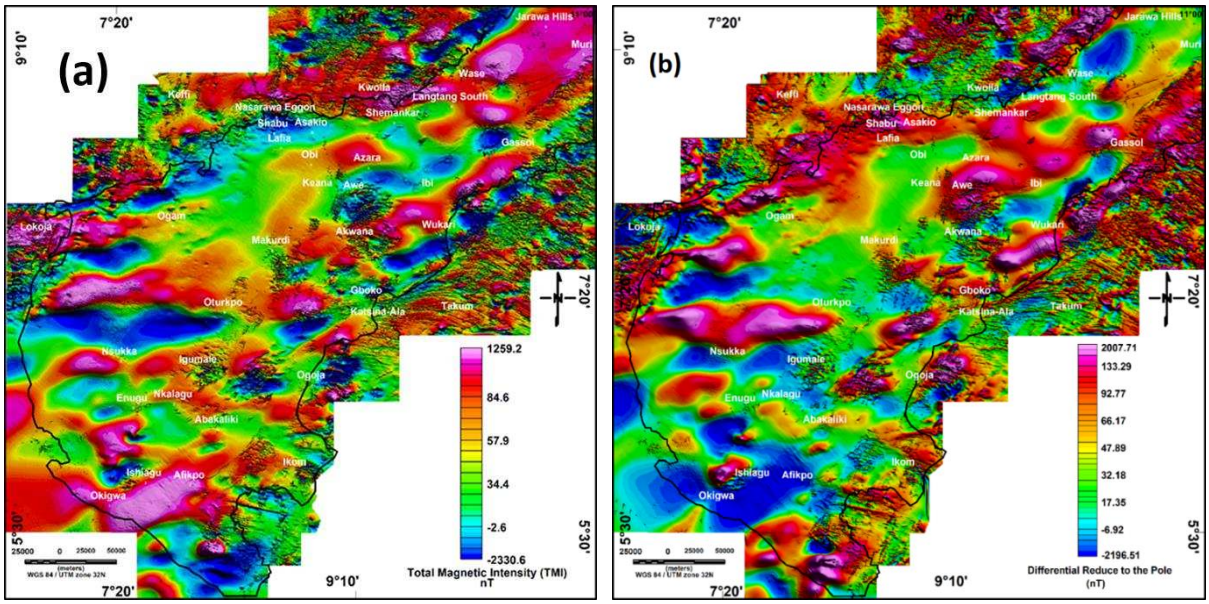

Fig. 3: (a) Total Magnetic Intensity (TMI) map has been colour-filled and histogram equalized. (b) Differential reduction to the pole (DRTP) of TMI.

4. Results and interpretations

4.1 2D gravity and magnetic models across the Trough

We carefully applied 2D gravity and magnetic modelling techniques to investigate the presence of structures and geological features both within sediments, on and below the basement (Vargas et al., 2015; Ghazala et al., 2018). Modelling was performed using GM-SYS^{TM} version 9.8 for both magnetic and Bouguer anomaly data sets. The gravity/magnetic response of the model was estimated and compared with the observed profiles and the model was modified to fit the response between the calculated and the observed values. Four (4) cross-sectional profiles were drawn across the trough in the NW-SE trend direction, perpendicular to the NE-SW main structural trend direction (Figs. 4 a and b). Profiles MBT1N and MBT2N are located in the Middle Benue Trough while MBT3N and MBT4N are in the Lower Benue Trough. It is important to mention that this modelling technique is non-unique i.e., many geometric/geological models will fit the gravity or magnetic data and as such, we incorporated available constraints, as well as geological and structural knowledge of the area (Tulyatid and Fairhead, 1996; Geosoft Inc., 2009; Aboud et al., 2015). However, in this study, we reduced the level of ambiguity by modelling both gravity and magnetic datasets along the same profile.

Three main geo-structural morphologies were modelled across all the profiles; the basement architecture, the Curie isotherm, and the Moho interface. The Curie isotherm was modelled by incorporating the knowledge gained from the spectral technique in estimating the regional Curie depth of the area (Bello, et.al, 2017; Nwankwo and Sunday, 2017; Yenne, 2022). We estimated the average depths along profile MBT1N for the top to basement, Curie, and Moho interfaces as 4.30 km, 16.50 km, and 18.78 km, respectively (Fig. 5 a). The mantle is observed to be uplifted and the crust thinned beneath the basin. Generally, the thinning of the crust is an indication of extension or stretching of the crustal materials during rifting. This geometry of the crust may be due to pure shear with associated normal faults. The geologic model across profile MBT2N gave an average depth of 7.62 km for the basement, 13.30 km for Curie depth, and 17.30 km for Moho (Fig. 5 b). We observed high positive gravity anomaly values at the centre and at the far SE part of the area. These anomalies were modelled to be as a result of the presence of mantle uplift and volcanic rocks/plugs. There is a relatively flat Curie depth interface and we interpreted it to be due to the cooling of the crust over time. The geologic section indicated that the crust has been well stretched, thinned, and extended, and could be associated with pure shear tectonics. Profile MBT3N showed a mean depth of 7.10 km for the basement, 13.45 km for the Curie depth, and 17.08 km for the Moho (Fig. 6 a). We observed and modelled the emplacement of supracrustal volcanic rock with a possible crater towards the right end of the basin due to the presence of two peaks of high gravity anomalies. The mantle is slightly uplifted here with an average depth of 17.08 km. The crust is slightly thinned but thickens towards the end of the basin. Profile MBT4N indicated an average basement depth of 7.50 km while the Curie depth remained relatively the same at an average of 13.10 km as of MBT3N (Fig. 6 b). An emplaced volcanic block was also observed towards the right edge of the profile that peaked at about 100 mGal. The Moho has a maximum depth of 19.02 km, indicating a slight stretching and thinning of the crust. Generally, the geologic model indicated

that the Curie depth is shallower than the Moho interface indicating that the crust is likely to be continental in nature.

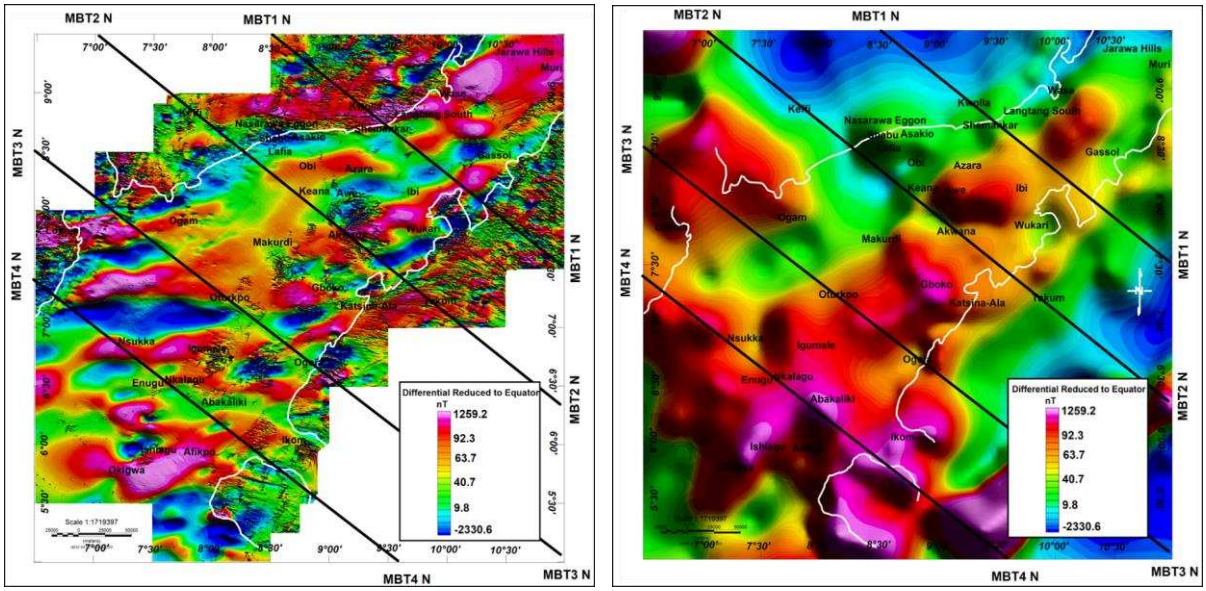

Fig. 4: (a) Magnetic map (b) Bouguer anomaly (Gravity) map. Four profile lines perpendicular to the general trend direction of the trough run NW-SE.

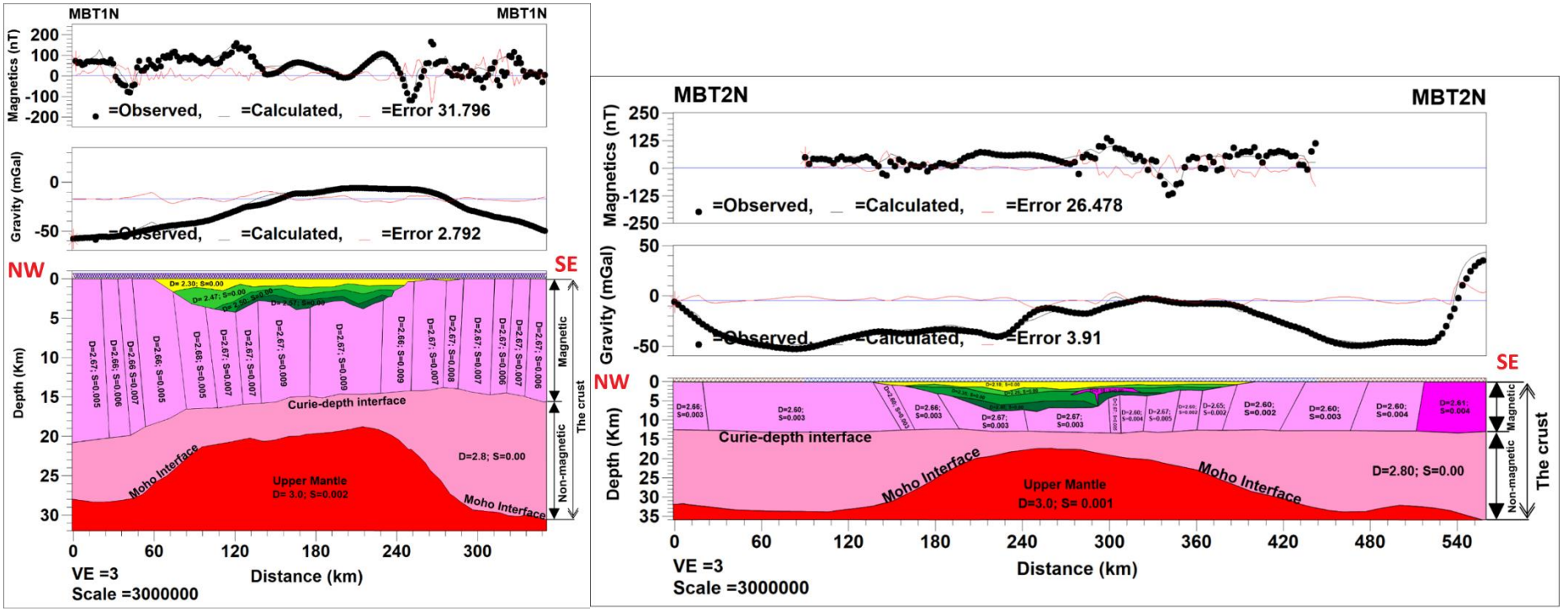

(a) (b)

Fig. 5: 2D gravity and magnetic geologic model for Middle Benue Trough along profile (a) MBT1N with a total length of 350 km. (b) MBT2N of length of 560 km. The top, middle and bottom sections show observed and calculated magnetic and gravity anomalies, and the geologic model, respectively. D, S and VE are density (g/cc), susceptibility (SI), and vertical exaggeration, respectively. The profiles do have the same scale.

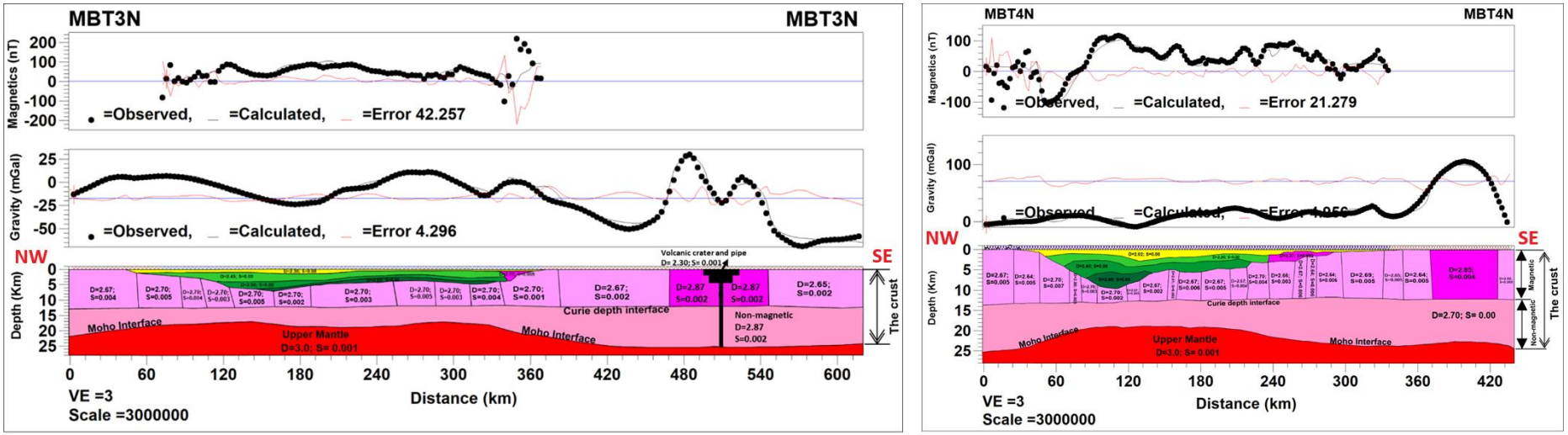

(a) (b)

Fig. 6: 2D gravity and magnetic geologic model for Middle Benue Trough along profile (a) MBT3N of length of 626 km. The double peak at the right side of the profile is due to a volcanic pipe and crater with lower density materials (volcaniclastics and local sediments) acting as a conduit through which magmatic materials are emplaced. The magma chamber (black polygon) may be empty or contains volcanic ash that is relatively lower in density than its surrounding volcanic rocks. (b) MBT4N of length 436 km. Basement depth, Crustal thickness variation, Moho geometry, Curie depth and sub-basin mapped. The top, middle, and bottom sections are magnetic and gravity anomalies, and the geologic model, respectively while D, S, and VE are density (g/cc), susceptibility (SI), and vertical exaggeration, respectively.

4.2 Basement mapping

4.2.1 Basement faults

A plot of the averaged power spectrum of the DRTP map (Fig. 3b) was used to determine the average depths to different magnetic contributions based on their wavelengths (Ali *et al.*, 2017). We differentiated the attributes according to their average depth locations into shallow and deep anomalies or structures (Spector and Grant, 1970; Hinze et al., 2010; Ali et al., 2017). Three main depth slices were obtained: Depth slices 1, 2, and 3, representing the residual (shallow), intermediate, and regional (deep) sources, respectively (Fig. 7). Depth slice 1 (800-3700 m wavelength) is at a shallow mean depth of 245 m, dominated by very short wavelengths due to the presence of surface noise, cultural features, and surface igneous rocks. The intermediate depth slice 2 (3700 - 15500 m wavelength) is at an average depth of 1210 m composed of intermediate wavelengths attributed to supracrustal volcanic materials, plugs, dykes and bosses, etc (Fig. 8 a). Depth slice 3 (15500 m and longer wavelengths) is located at a mean depth of 7780 m that is dominated by the presence of long wavelengths or regional anomalies due to deep magnetic bodies and other crustal structures (Fig. 8 b). This depth slice (regional anomalies) was used in mapping the presence of faults on the basement.

The regional anomalies are those dominated by long wavelengths and related to deep sedimentary and basement structures (Ali *et al.*, 2017). Derivative-based or edge detection techniques (horizontal gradient magnitude and tilt) were used to delineate edges of deep basement faults (Fedi and Florio, 2001; Li et al., 2010; Fig. 9). 9 (a) shows the maxima of horizontal gradient magnitude indicating the presence of basement lineaments (faults). The horizontal gradient is less sensitive to noise and gives more precise and clear structural boundaries, thereby avoiding the production of additional structures that are not important (Pham, 2024 a; Pham, 2024 b). The zero of the Tilt angle is marked on the Tilt map to delineate the edges of linear structural features interpreted as basement faults (Fig. 9 b). The results of the lineament analyses from regional magnetic anomalies were combined to represent the deep faults and overlain on the positive tilt angle (Fig. 10 a). The slope direction of the tilt angle across the edges of the faults shown by a tick indicates a lower tilt value or low magnetic susceptibility (Fairhead et al., 2011; Ali et al., 2017). The direction of the tick pointing towards lower susceptibility can be interpreted as the downthrown side of the fault while the positive tilt angle values as the upthrown side (Fig. 10 a). A combination of results from mapping structural edges (lineaments) referred to as basement faults/contacts indicated three major trend orientations of NE-SW, NW-SE, and ENE-WSW (Fig. 10 b). Analyses of the basement faults show that the NE-SW faults are dominant in the area. However, the process of correcting the distortion of simple RTP by the DRTP transformation with pseudo-inclination has suppressed the N-S trending structures, hence, they were not mapped.

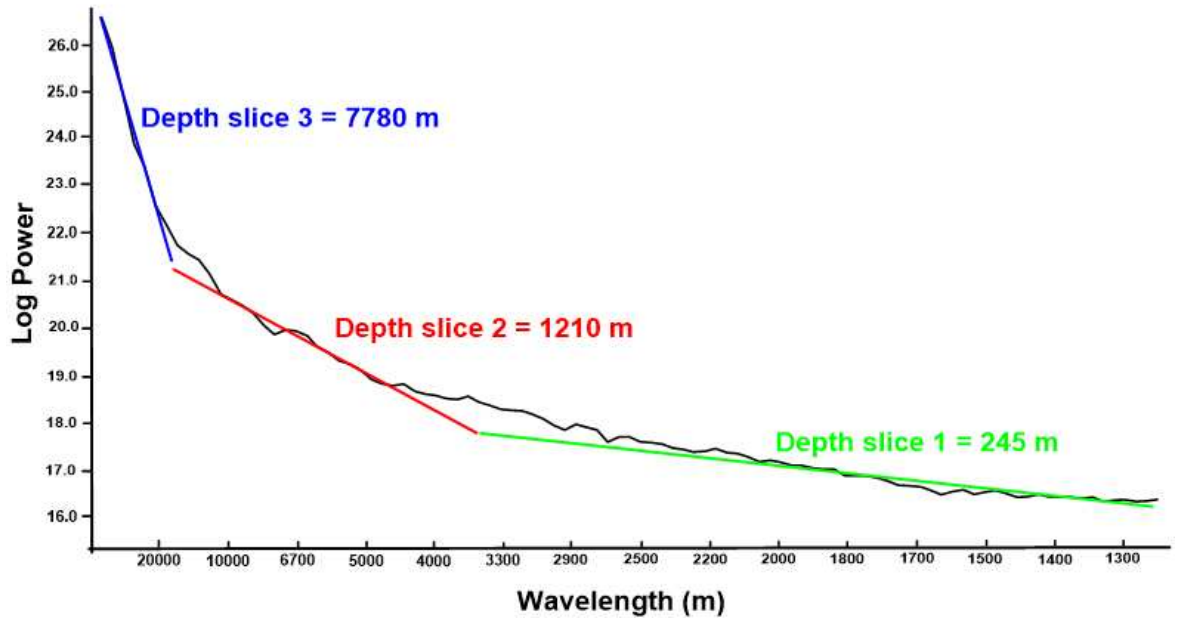

320

321 **Fig. 7: A power spectrum analysis of the DRTP anomaly map matching three distinct**
322 **pseudo-depth slices. Three (3) average depth slices are identified.**

323

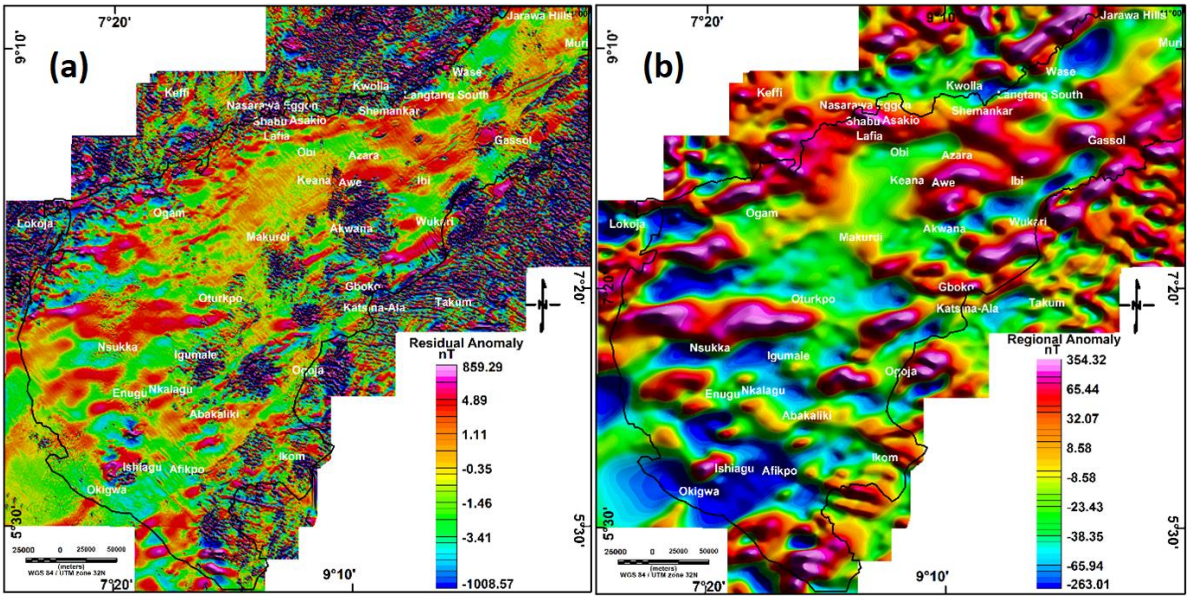

324

325 **Fig. 8: Aeromagnetic data (a) Depth slice 2 corresponds to the short wavelengths of the**
326 **shallow geologic features (Residual anomaly map) (b) Depth slice 3 corresponds to**
327 **the deepest equivalent layer at depth 7.8 km which could be as a result of basement**
328 **morphology and other deep crustal geologic features. Depth slice 1 is not presented,**
329 **but is mostly noise.**

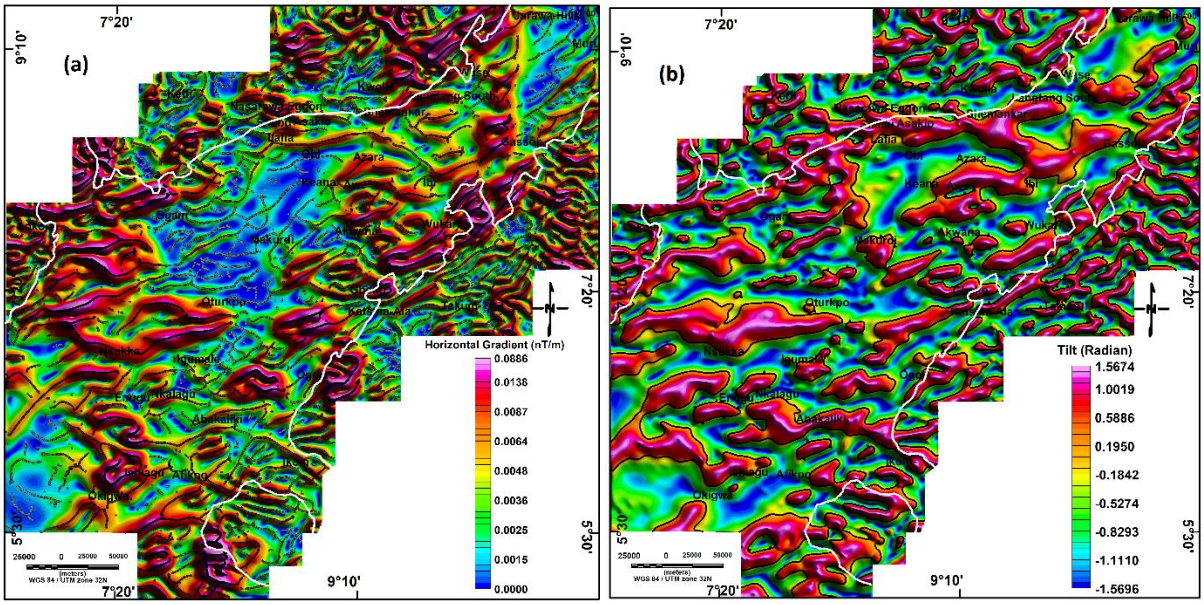

330

331 **Fig. 9: Basement lineaments extracted from regional DRTP (a) Horizontal gradient with**
332 **maxima (black dots) overlaid to show the edges of structures (b) Zero of tilt angle**
333 **(black line) marked on tilt angle map.**

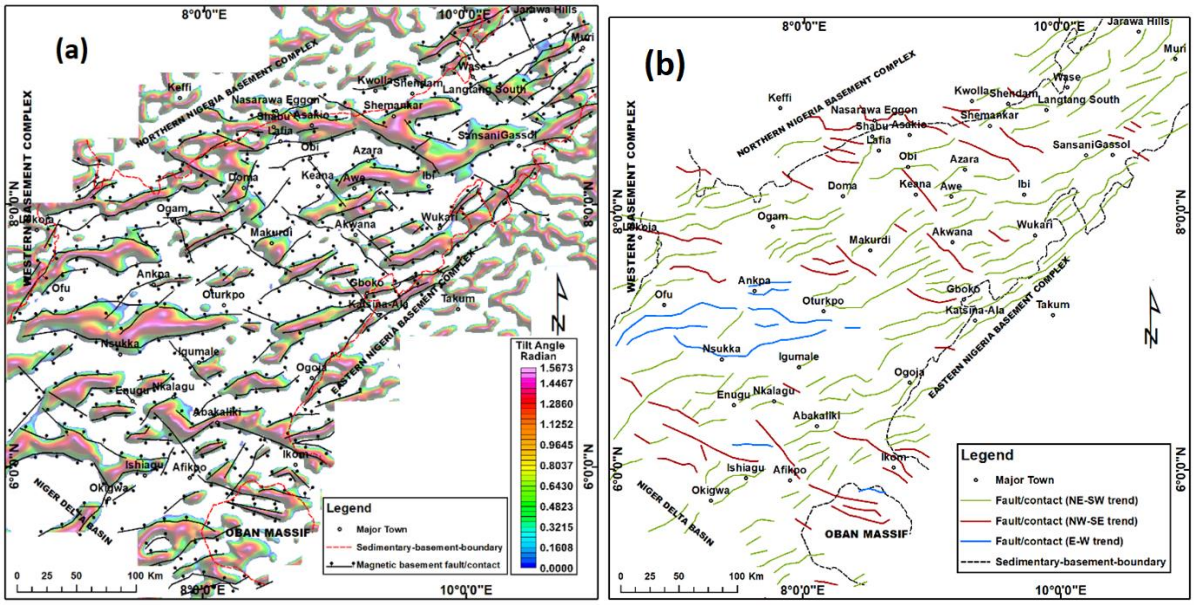

334

335 **Fig. 10: (a) Basement faults overlay on positive tilt angle obtained from the regional**
336 **DRTP. The ticks show the direction of lower magnetic susceptibility (possible**
337 **downthrown sides of the faults from the delineated structural edges. (b) Interpreted**
338 **basement fault map with three main structural trends; NE-SW (green), NW-SE**
339 **(red), and ENE-WSW (blue) orientations.**

340

341

342

4.2.2 Basement depth estimation

The DRTP map (Fig. 3 b) was transformed into the pseudo-gravity field in the Fourier domain such that the resulting field resembled gravity data, but based on susceptibility variation - following the approach of Salem et al., 2014. We scaled the vertical integration of DRTP to the pseudo-gravity field making it suitable for inversion as though it were a gravity anomaly map (Salem et al., 2014; Geosoft Inc., 2015; Fig. 11 a).

We avoided using Bouguer anomalies due to difficulties in differentiating between the gravity effects of deep sediments and shallow Moho. We do not have borehole or seismic data to constrain the inversion. Pham et. al. (2018) estimated basement depth directly from gravity data using the prior information of the densities from an available drill-hole data. The depths to the top of the basement estimated from 2D gravity and magnetic models (Figs. 5 and 6) were used to constrain and calculate susceptibility contrast based on the infinite Bouguer slab formula (Salem *et al.*, 2014). The pseudo-gravity map enhanced deep magnetic anomalies (long wavelengths) corresponding to basement anomalies and enabled the estimate of depth (Fig. 11 a). The adjusted pseudo-gravity dataset was used for the 3D inversion. A MATLAB source code 3DINVER.M written based on the Parker–Oldenburg approach (Oldenburg, 1994; Parker, 1972; Gómez-Ortiz and Agarwal, 2005) was employed for the depth estimates.

The adjusted pseudo-gravity data set was inverted based on a mean basement depth of 5.5 km and susceptibility contrast of 0.004770 (cgs), based on profile models and the results of Obaje, 2009 and Anudu *et al.*, 2020. The inversion produced a basement depth relief map with an average depth of 6.54 km and an RMS value of 0.0017 with 2 iterations (Fig. 11 b). The magnetic bodies in the trough are generally a bit deeper than those in the surrounding area indicating that the sediments themselves are non-magnetic. Generally, a maximum basement depth of 9 km and minimum depth of 4 km was obtained. The basement relief shows areas of basement uplift and subsidence in different parts of the trough. It showed significant basement uplift in the Northern part (Middle Benue Trough), particularly around Awe-Azara and Gassol towns. A major NW-SE trending basement uplift between Shemankar and Ibi and a NE-SW trending ridge-like feature is observed between Gboko and Wukari. Basin subsidence (sub-basins) is observed around Wase-Jarawa Hills, Lafia-Asakio-Keana, Akwana-Ibi-Wukari, and Makurdi axes. In the southern part of the area (Lower Benue Trough) are also several basement uplifts including Ogoja-Katsina-Ala, Ishiagu-Okigwa, Nsukka-Oga axes while the Afikpo-Enugu-Okigwa, Nkalagu-Igumale-Oturkpo, Lokoja axes show the presence of subsidence.

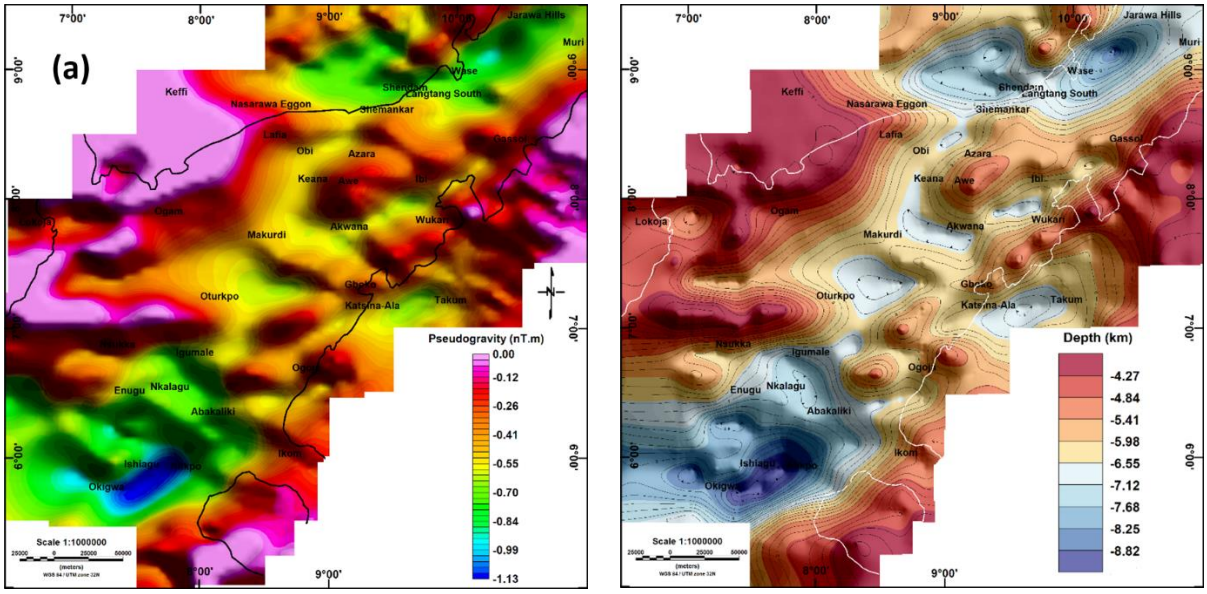

Fig. 11: (a) Pseudo-gravity map derived from the DRTP. It has been adjusted so that all values are less or equal to zero (0). (b) 3D depth to the basement map. The mean terrain clearance of 80 m has been removed.

4.3 Curie depth estimation

We modelled the susceptibility of magnetic bodies within the basin and determined the depth to the bottom of the magnetic source (a good proxy for the Curie depth estimation) using a 3D inversion technique. The approach used assumes that the anomalous magnetization direction is the same as the direction of the earth's field – i.e. no remanent magnetization (Li and Oldenburg, 1996; Macleod and Ellis, 2013; Mickus and Hussein, 2016; Arkani-Hamed, 1988; MAG3D, 2017). We discretize the area using a cuboid mesh with lateral extent corresponding to the study area and dimensions of 500 km X 500 km containing 50 (1 x 1 km) cells in both the easting and northing directions and a fixed vertical depth of 50 km with 50 cells of 1 km thickness. Mag3D v6.0 package was used to invert the TMI dataset directly (Li and Oldenburg, 1996). The resulting geologic model shows in 3D the magnetic susceptibility contrast block with the distribution of magnetic susceptibility across the basin in-depth, hence, defining materials that are magnetic and those that are not (Fig. 12). The result shows highly magnetic bodies in the south and east of the area which are probably associated with volcanic rocks; other magnetic rocks probably mostly represent the basement.

Furthermore, the 3D magnetic susceptibility distribution block was investigated by depth slicing across four (4) profiles. The result shows several components of magnetic bodies within and without the trough and allows the estimate of the Curie depth points as a line below the most significant magnetization shown in the inversion (Fig. 12). The cross-section across profile L1-L2 indicates three (3) main geologic bodies identified as A, B, and C with estimated average Curie depth points (CPD) of 16.6 km, 16.5 km, and 17.5 km, respectively (Fig. 13 a). Profile L3-L4 cross-section shows four (4) main isolated magnetic anomalous sources A, B, C, and D with estimated CPD of 11.1 km, 17.1 km, 16.9 km, and 18.0 km, respectively (Fig. 13 b). Fig. 13 c shows the cross-section across profile L5-L6 where the average CPD of the magnetic body A is 17.1 km while magnetic body B is 18.5 km. Geologic model across profile L7-L8 indicates magnetic bodies A and B with CPD of 18.3 km and 16.5 km, respectively (Fig. 13 d). In each of the cross-sections, the Curie depth interface was identified and beyond this point, rocks are assumed to be non-magnetic (above Curie temperature 580 °C) (Hsieh et al., 2014; Speranza et al., 2016). Generally, the geologic model indicated decreased magnetic susceptibility showing the limit or bottom of isolated magnetic sources or the Curie depth interface. The Curie depth estimated from this technique largely agrees with those estimated from the 2D models.

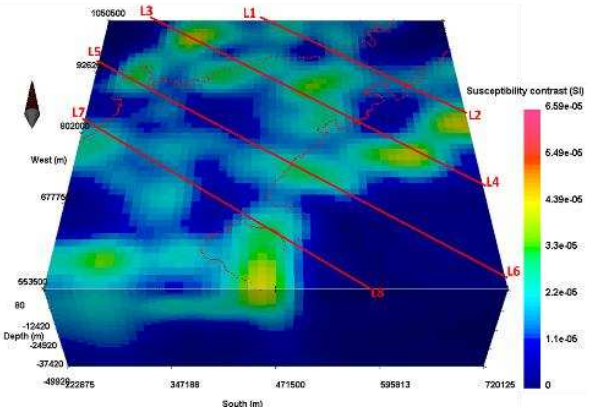

Fig. 12: 3D magnetic susceptibility block showing four (4) profiles across the basin.

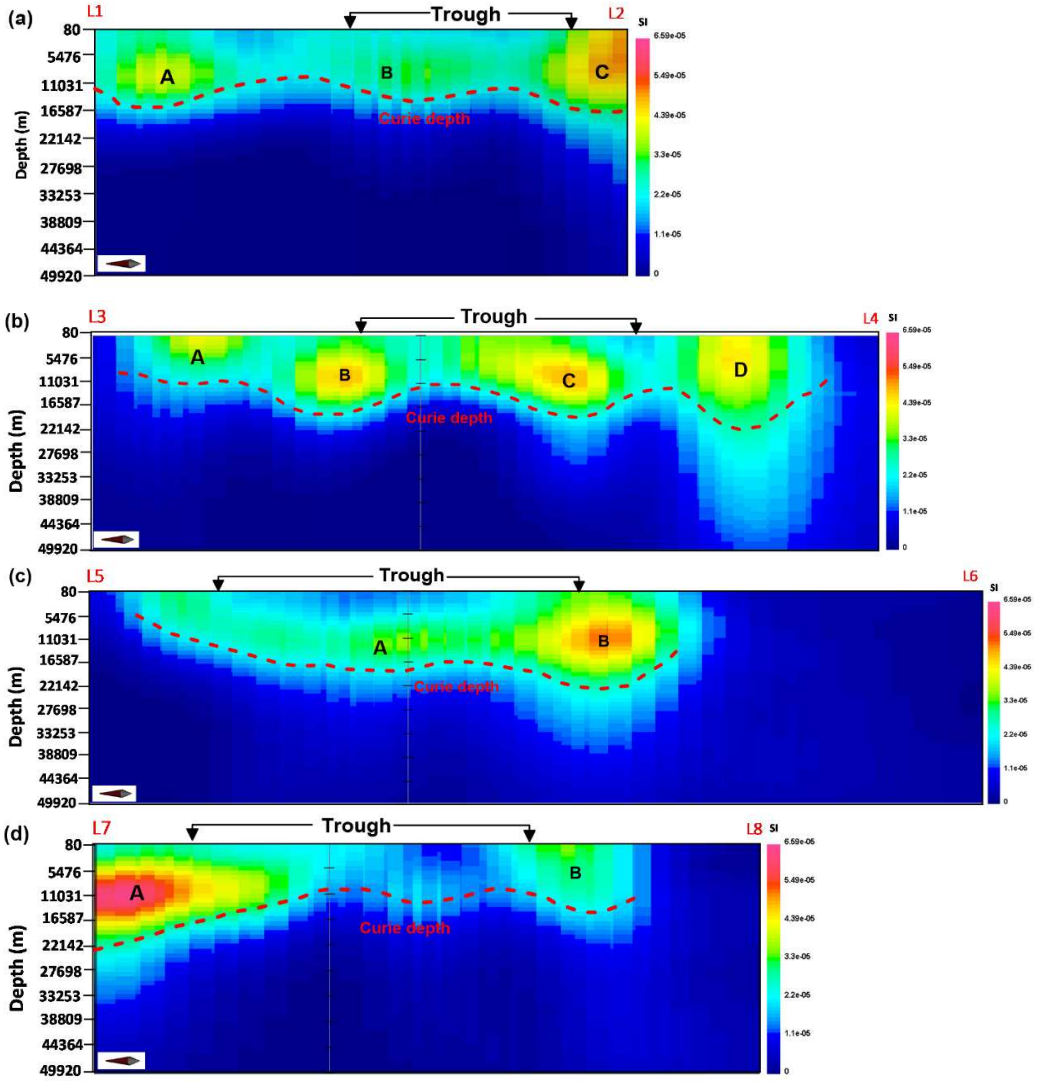

Fig. 13: (A) 3D magnetic susceptibility cross-sections across profile (a) L1-L2. A and C are from surrounding rocks while B is within the basin with lesser magnetic susceptibility (b) L3-LT4 with C found within the basin. (c) L5-L6 where A is found within the basin while B is part of the surrounding rocks. (d) L7-L8. A and B are found at the boundary of the basin. No significant magnetic body with the basin. All sections have vertical scale exaggeration (VE) of X 3 while the horizontal axis is not to scale.

462 **4.4 Moho morphology mapping**

463 We estimated the depth and mapped the morphology of Moho using a 3D inversion technique.
464 Gravity inversion of Bouguer anomaly (Fig. 4 b) was employed to generate the 3D density
465 anomaly model with the aim of mapping the Moho interfaces using depth to the basement map
466 as constraint (Welford and Hall, 2007). We applied the Li-Oldenberg inversion approach that
467 involved the use of a GRAV3D inversion algorithm and allows the incorporation of *a priori*
468 model information to produce a targeted result (Welford and Hall, 2007). This algorithm inverts
469 gravity observations at the Earth's surface (Bouguer anomaly) to obtain a subsurface 3D
470 density anomaly below the observation point relative to background density (Li and Oldenburg,
471 1996 and 1998). In carrying out the inversion process, a mesh was constructed from flattened
472 cubes with lateral extent corresponding to the study area and dimensions of 10 km X 10 km
473 containing 50 cells in both the easting and northing directions. The vertical depth of 35 km was
474 chosen to give the best result after testing several vertical depth extents (25 km, 30 km, and 40
475 km); it was divided into 50 cells of thickness 700 m. We then built a reference density model
476 that holds *a priori* geophysical information, i.e., the depth to basement map (Welford and Hall,
477 2007, Welford et al., 2010; Deng et al., 2014). The model was assigned sedimentary densities
478 to the top of the basement, i.e., using the basement map from Fig. 11 b. The inversion algorithm
479 for the sediments was modified such that the density anomaly within a given prism was only
480 allowed to vary between -0.76 g/cc and 0.247 g/cc density contrast, and controlled by the depth
481 to the basement. This has ensured that features of known density are incorporated directly into
482 the reference density anomaly model and the remaining cubes below the basement were
483 unaffected during the inversion. Hence, all the remaining mesh prisms below the top of the
484 basement were given a 0.00 g/cc density anomaly conforming to the background density
485 anomaly; the density anomaly in each of these prisms could vary between -1.00 g/cc and 1.00
486 g/cc density contrast for the whole area; i.e., the density ranges between 1.60 g/cc and 3.60
487 g/cc (average host rock density 2.60 g/cc). This allowed for great freedom in inverted density
488 anomalies below the sediments to reproduce the observed gravity effect. Also, given the fact
489 that gravity data has no inherent depth resolution and may lead to the concentration of density
490 anomalies near the earth surface (Li and Oldenburg, 1998), a depth weight function was
491 constructed and applied so that all cubes at all depths were considered during the inversion
492 (Welford and Hall, 2007; Cella and Fedi, 2012). The observed gravity anomaly map (Bouguer
493 anomaly) of the area was inverted directly by the GRAV3D software to produce a 3-D density
494 structure of the area.

495 The inverted density model showed two (2) layers (the crust and upper mantle) below the
496 basement surface. We studied the basin using four (4) profiles (L1-L2, L3-L4, L5-L6, and L7-
497 L8) in 2D cross-sections to understand the crust and the Moho interface (Fig. 13). Figs. 14 a
498 and b show 2D cross-sections along profiles L1-L2 and L3-L4 with interpreted crust, Moho,
499 and upper mantle identified. The Moho is uplifted underneath the basin where there is high
500 gravity response. The high gravity anomaly could be attributed to the injection and
501 emplacement of high-density magma materials within and on the basement rocks or the crust.
502 These models indicated that there is crustal stretching leading to thinning and upwelling of the
503 mantle with associated block faulting and subsidence (McKenzie, 1978). Figs. 14 c and d are

the 2D cross-sections along profiles L5-L6 and L7-L8 that show the crust, Moho, and Upper Mantle also. Moho elevation is not prominent but very gentle and subtle just as observed from the 2D gravity/magnetic models. The right-hand ends of these profiles indicated an increase in crustal thickness due to the presence of magmatic materials. Generally, all the cross-sections showed and differentiated effectively the crust and the mantle. The fit between the observed and predicted or calculated gravity anomaly is very good, thereby validating the 3D block model and the technique. The Moho depth of the Trough ranges between 20.8 km and 35.1 km.

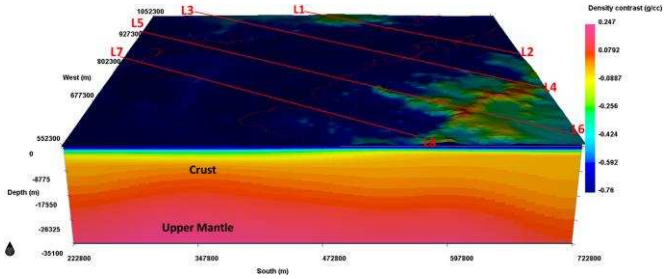

Fig. 14: 3D inverted density model showing four (4) profiles. Two (2) major density units are observed, i.e., indicating the crust and the upper mantle.

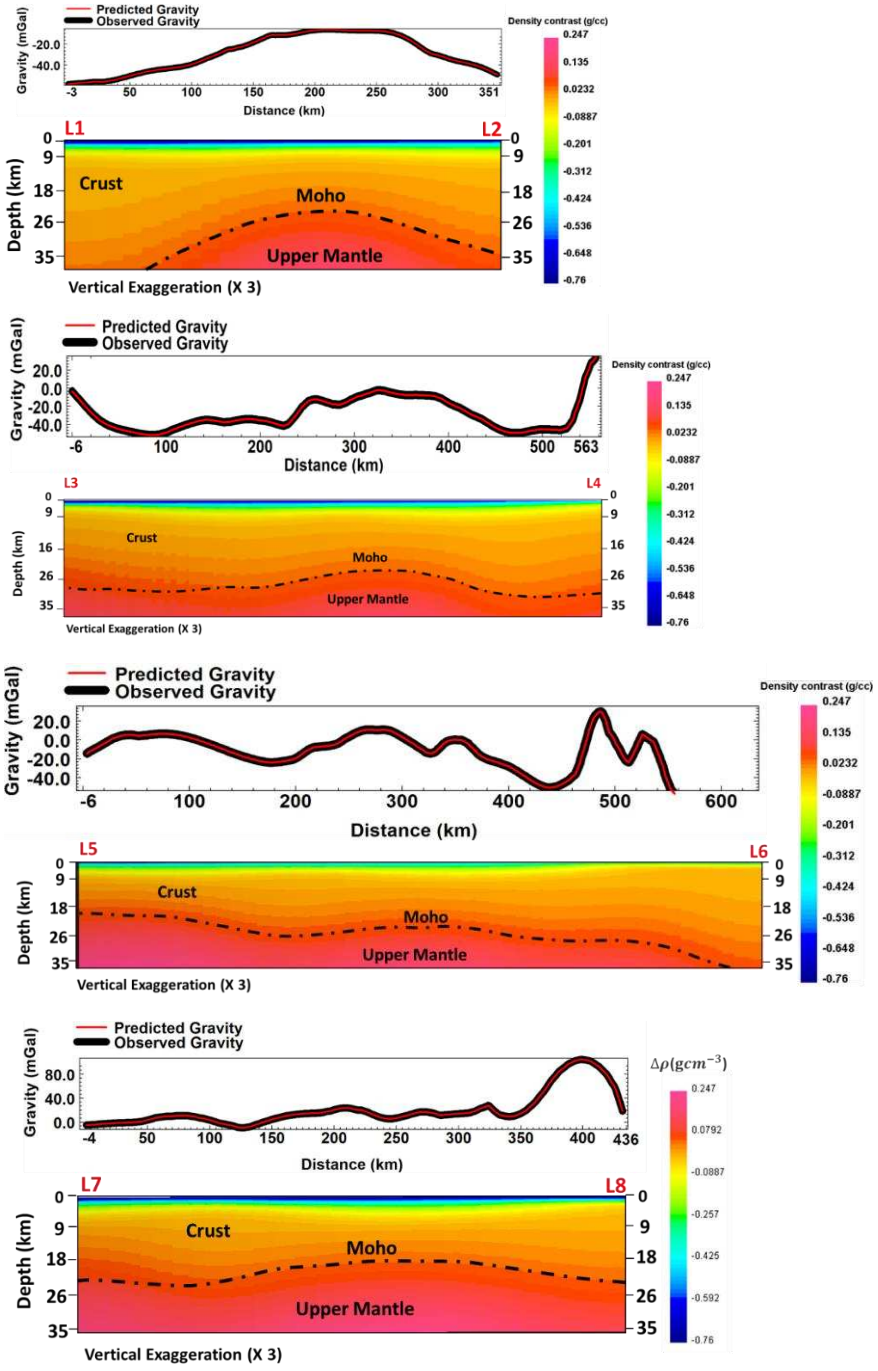

Fig. 15: 2D cross-sections along profiles showing the crust, Moho, and upper mantle. The Moho is uplifted within the trough.

5. Discussions

5.1 Sedimentary thickness map

Several basement lows were identified from the sedimentary thickness map with depths that are greater than 6 km. The basement lows are interpreted as sub-basins and are suitable sites for the accumulation of sediments (depocentres). Basement highs are also found in many parts of the trough with depths less than 2 km especially in the northern part (Middle Benue Trough) and between 2 and 4 km in the southern part (Lower Benue Trough). These basement highs are found to be associated with high magnetic susceptibility values probably due to magmatic intrusions within or on the basement occurring close to the earth's surface (Fairhead, 2015). Examples of areas of basement uplift with high magnetic susceptibility are found around Awe-Ibi and Ishiagu, Nsukka-Ankpa. A major E-W basement high is observed in the southern part (around Nsukka) which may probably be a horst-like structure that has been detached by the E-W detachment fault.

5.2 Fault kinematics from basement faults

The spatial spread of basement faults in the area showed three main orientations (NE-SW, NW-SE, and the ENE-WSW trends), which we believe are indications of the different periods of tectonic activity that affected the Trough over time (Fig. 16 a). They also give an idea of the deformation pattern of shallow and deep-seated crustal rocks. We applied fault kinematic and paleo-stress field analyses to predict their evolution pattern and time of formation.

The NE-SW trending faults are the most dominant and form en-echelon sets that run parallel to the main trend of the trough. They correspond to the orientation of the basin-bounding faults associated with the Aptian rifting and the regional sinistral kinematics (Guiraud and Maurin, 1992). These faults are believed to have evolved due to rifting that started in the Early Cretaceous (Aptian; 142-120 Ma) where the regional maximum extensional stress was approximately NNW-SSE (Guiraud and Maurin, 1992; Fairhead et al., 2013; Fig. 16 b), thereby creating the NE-SW trending extension-dominated normal faults with some strike-slip components. This is possible when the σ_3 is assumed to act horizontally while σ_1 is vertical (Fig. 16 b). These faults seem to accommodate most of the crustal extension during rifting. The regional maximum extensional stress (NNW-SSE direction) is believed to have enabled the development of the ENE-WSW trending normal faults during the late Aptian when the extensional stress acted more in a N-S direction (Ajakaiye et al., 1991; Guiraud and Maurin, 1992; Fig. 16 c). They correspond to further change in the stress field orientation of the regional trend experiencing a wrench or pull-apart motion due to relative movement of the NW Africa sub-plate to the SW (Fairhead *et al.*, 2013). They are found mainly in the southwestern part and seem to control major tectonic activities (uplift and down-warping) and enabled the scissors-style opening geometry of the Lower Benue Trough. The NW-SE striking faults are interpreted to have initially formed during rifting in the Albian (Fairhead *et al.*, 2013). They are believed to have evolved during the Albian (119-101 Ma) as a result of the effect of the regional sinistral strike-slip movements associated with the Central African Rift System (CARS) tectonics (Fairhead and Green, 1989; Guiraud and Maurin, 1992). The NW-SE normal fault kinematic is such that both the intermediate and the minimum stress axes are horizontal

with the principal extensional stress axes acting parallel to the regional sinistral strike-slip direction i.e., NE-SW direction and the maximum stress axis acting vertically (Fairhead and Binks, 1991; Fig. 16 d). This proved that there was a change in the orientation of the principal extensional stress axis from NNW-SSE to NE-SW i.e., giving it a dextral sense of movement but showing a form of sinistral kinematics along the NW-SE faults. The NW-SE trending faults are perpendicular to the NE-SW trends.

Reversal of the stress pattern from the extensional stress field to a compressive stress field resulted in the reactivation of most of the basement faults during the Late Santonian (84 Ma). Here, the least compressive stress axis acts vertically (Guiraud and Maurin, 1992, Mamah et al., 2005). This reversal in stress fields led to basin inversion and deformation of pre-existing sedimentary rocks through the NE-SW, NW-SE, and ENE-WSW basement faults (Binks and Fairhead, 1992; Fairhead et al., 2013). It is important to mention that fault reactivation is most likely to have favoured basin inversion in the area since it requires less energy than any other factor (Fairhead and Binks, 1991; Lowell, 1995; Guiraud and Bosworth, 1997; Mamah et al., 2005). The Santonian event led to the compression of some of the deposited sediments resulting in the creation of folds and uplift of basement blocks, thereby creating anticlinal and synclinal structures with NE-SW striking axial traces (Fairhead and Green, 1989; Guiraud and Bosworth, 1997; Fairhead et al., 2013). The presence of the basement fault network, basement uplifts, and sub-basins covered by thick sedimentary rock indicates the hydrocarbon potential of the area (Obaje *et al.*, 2006; Abubakar, 2014). These faults trends and characteristics agree to a great extent with the structural trends reported by many authors (Anudu, et al., 2014, Oha et al., 2016; Abdullahi et al., 2019). The fault types control the geometry and alignment of the sediments of the basin and are significant in restricting the emplacement patterns of magmatic material as well as the location of mineral deposits. Generally, the Middle Benue Trough shows a small sedimentary thickness which gradually increases to the south. The thickest sediments are found around the southern part of the area toward the Niger Delta.

5.3 Crustal structure of the basin

The crustal structure for the basin was obtained from 3D basement depth and 3D Moho estimates (Figs. 11 b and 15, respectively). The crust is observed to be stretched and thinned across the trough and the amount of stretching increases from north to South. Crustal stretching and extension combined with Moho uplifts are believed to have caused crustal thinning observed directly beneath the centre of the trough. The southern part of the trough has a thinner crust than the northern part with the smallest crustal thickness of about 9 km in the south compared to 13 km in the north (Fig.17 a). The southern part of the area has a larger stretching factor than the northern part. It is known that extension of continental lithosphere may generate melts of alkali basalts and tholeiites when the amount of stretching is great (Mckenzie and Bickle, 1988). It can be implied that the source of the magma emplaced and modelled within the trough is from mantle materials as areas of shallow Moho correspond to zones of magmatic activity. The areas that show high mantle uplift could be interpreted as areas of shallow Curie depth which implies that the lithosphere has been stretched and hot material has been brought to shallower depth thereby increasing the temperature of the surrounding host rock. Large amounts of magma is believed to have been emplaced along the Cameroon volcanic line in the

eastern part of the area and along the Jos volcanic line in the North-western part of the area (Ajakaiye and Burke, 1973; Deplaen et al., 2014). These areas of shallow Moho also correspond to the areas of crustal thinning and shallow Curie depth. The shallow Curie depth is mainly towards the eastern part of the trough where the magmatic intrusion is prominent (Jiménez-Díaz *et al.*, 2014).

5.4 Hydrocarbon exploration potential and prospectivity

The Benue Trough has similar structural and tectonic events to the Muglad basin in Sudan and South Sudan and the Termit basin of Chad and Niger where commercial hydrocarbons have been discovered (Obaje et al., 2006; Abubakar, 2014). Hydrocarbon exploration within the trough has been carried out in the Upper Benue Trough; Kolmani River-1, Kuzari-1, and Nasara-1 exploratory wells have total depths of 3 km, 1.5 km, and 2 km respectively (Obaje et al., 2004; Obaje, 2009; Habib and Xie, 2012) while recent exploration for oil and gas was carried out in the Anambra basin of the Lower Benue Trough (Habib and Xie, 2012). This study indicated that basement subsidence provided good depocentres for the deposition and accumulation of thick sedimentary rocks of about 9 km while basement uplifted blocks have a thin sedimentary thickness of about 4 km (Fig. 17 b). Most of the sub-basins and the uplifted blocks form graben and horst structures and are observed to be bounded by deep-seated faults. Deep-seated faults have been shown to be good pathways for the migration of fluid, and can be oil-bearing if they occur together with an excellent trap system for hydrocarbons (Zbořil et al., 1986; Tulyatid, 1997; Cunningham and Mann, 2007).

Therefore, five (5) areas within the trough show the most favourable potential for hydrocarbon exploration based on some or all of the criteria above: Wase, Keana, Makurdi, Anambra, and Afikpo basins (Fig. 17 b). Rectangular block 1 located at the northern part of the area between Wase and Jarawa Hills is estimated to have a maximum depth of 9 km with the stratigraphy intact and fault-bounded, high heat flow and geothermal gradient and absence of a large amount of magmatic intrusive is interpreted to have high hydrocarbon potential. Block 2 has faults bounding established synclinal and anticlinal structures with high heat flow and geothermal gradient. The stratigraphy is well maintained with sediment thickness between 5 km and 6 km without basin inversion and magmatic intrusions affecting the sub-basin. This indicates the possibility of storing hydrocarbons. Several basement uplifts and areas of subsidence, interpreted as horsts and grabens respectively, are observed within block 3. The prospects for hydrocarbon exploration are high as the deepest depth is about 6 km and the shallowest has been up to 3 km. Blocks 4 and 5 have horsts and grabens, but also magmatic intrusion.

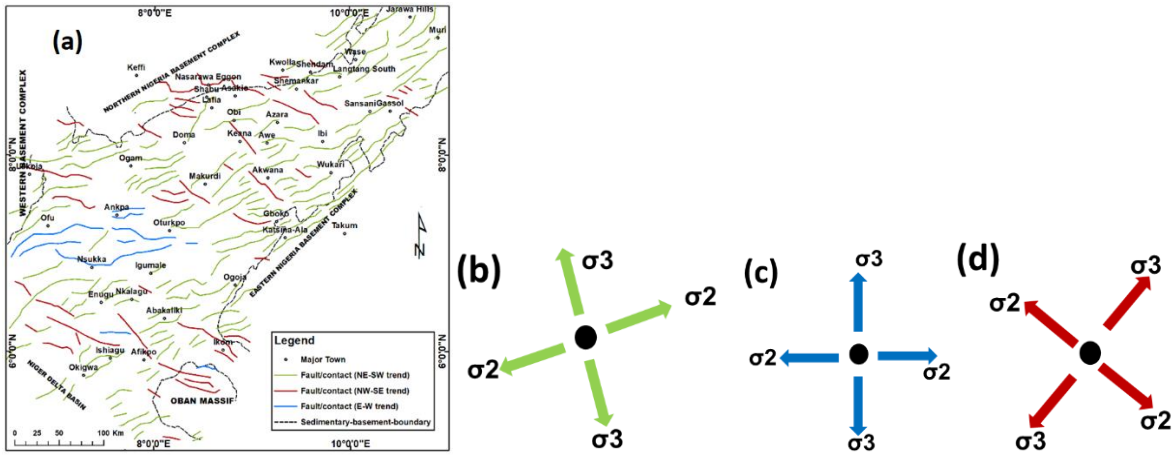

Fig. 16: (a) NE-SW, NW-SE, and ENE-WSW trending basement faults corresponding to normal faulting with some strike-slip component,b) Interpreted fault paleo-stress field orientation during rifting with the maximum extensional stress axis in approximately NNW-SSE direction in the Aptian leading to the formation of the NE-SW faults (c) Paleo-stress field orientation when the extensional stress axis is in approximately N-S direction during the late Aptian leading to the formation of the ENE-WSW faults (d) Paleo-stress field orientation forming the NW-SE trending faults (Albian) when the most extensional stress field is NE-SW due to advanced stage plate separation. Albian fault kinematics where the tectonic model indicates sinistral fault kinematics and a general dextral extensional movement.

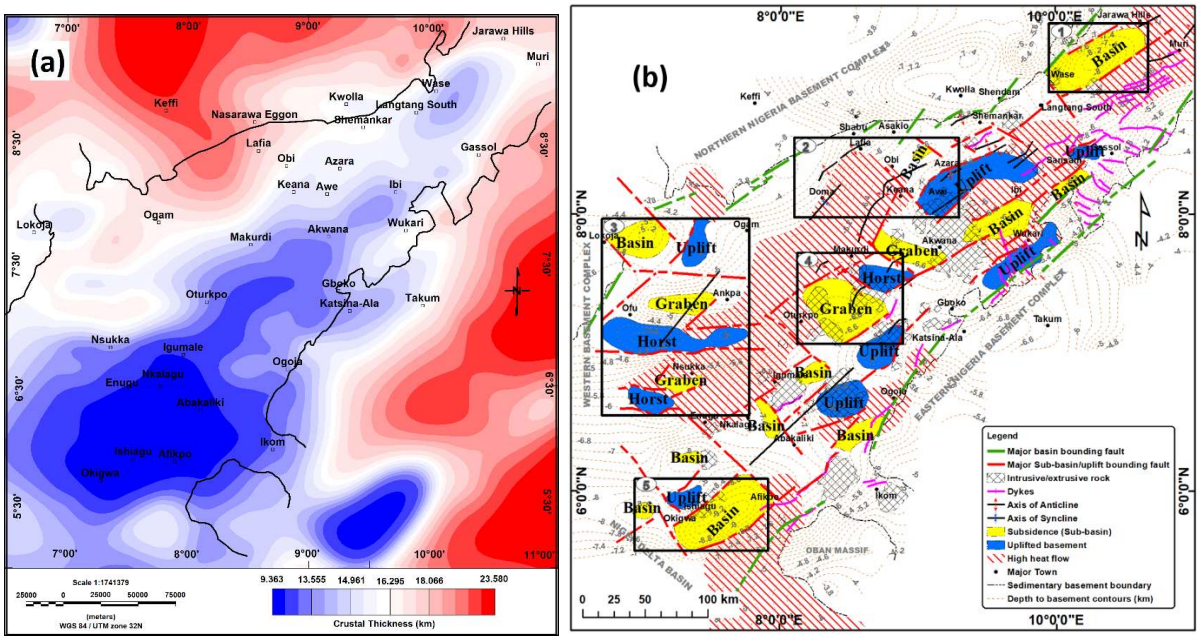

Fig. 17: (a) Crustal thickness map of the area with the crust thinned towards the centre due to stretching and mantle uplift (b) Hydrocarbon potential map of the Lower and Middle Benue Trough showing areas of high prospects for further exploration. The black rectangle blocks represent; 1: Wase Basin, 2: Keana Basin, 3: Anambra Basin, 4: Makurdi Basin, 5: Afikpo Basin.

5. Conclusion

This study confirmed three well-defined basement fault sets: NE-SW, NW-SE, and ENE-WSW faults. These faults are believed to be primarily normal faults and they control the main architecture of the basin tectonic activity. They are formed as a result of regional plate movements at different times and scales. We concluded that the NE-SW basement faults formed during the Aptian when the regional maximum extensional stress field acted in an approximately NNW-SSE direction while the ENE-WSW formed when the maximum stress field shifted to the N-S position during the Late Aptian. A further shift of the maximum extensional stress field to the NE-SW during the Albian led to the formation of the NW-SE basement faults. The basement is estimated to be at an average of 4.3 km from the ground level. Its morphology indicated areas of basement uplift typified by shallow depth values, and basement subsidence/sub-basins characterized by deep depths (depocentres) where thick sediments are accommodated. The uplifted basement blocks and sub-basins are identified to be fault-bounded and they control to a large extent the geometry of the trough. We modelled the Curie interface depth (the depth to the bottom of magnetic bodies) from 2D models to be relatively flat at an average of 13 km, while 3D inversion models estimated varied Curie depths that range from 11 km to 18 km. This depth interface is shallower than the Moho interface indicating the absence of oceanic materials emerging at the trough due to serpentinization and/or during continental break-up. The Moho is observed to be uplifted under the trough. We showed that the Moho in the Lower Benue Trough is deeper than in the Middle Benue Trough, and hence the reason for the presence of more magmatic intrusions at the Middle part. Our results indicated that the crust is thinned directly under the basin which we interpreted as the result of extensional rifting of the lithosphere leading to Moho doming and the emplacement of intrusive rocks. Finally, this study showed that the tectonic architecture of the trough is characterized by crustal rifting and extension, faulting, Moho uplift due to crustal thinning, magma emplacement, and thermal subsidence or relaxation. We concluded that our study agrees largely with the plate tectonic model for the evolution of the Benue Trough which elucidates the concepts of crustal rifting and extension, shallow Moho due to crustal thinning, magma emplacement, and thermal subsidence or relaxation.

References

Abdullahi, M., Singh, U.K. and Roshan, R, 2019. Mapping magnetic lineaments and subsurface basement beneath parts of Lower Benue Trough (LBT), Nigeria: Insights from integrating gravity, magnetic and geologic data, *Journal of Earth System Science*, 128(1), pp. 1–17. Available at: https://doi.org/10.1007/s12040-018-1038-9.

Aboud, E., El-Masry N., Qaddah, A., Faisal Alqahtani, F., Moufti, M.R.H., 2015. Magnetic and gravity data analysis of Rahat Volcanic Field, El-Madinah city, Saudi Arabia, *NRIAG Journal of Astronomy and Geophysics*, 4(1), pp. 154–162. Available at: https://doi.org/10.1016/j.nrjag.2015.06.006.

Abubakar, M.B, 2014. Petroleum Potentials of the Nigerian Benue Trough and Anambra Basin : A Regional Synthesis, *Natural Resources*, 2014(5), pp. 25–58.

Adighije, C.I,1981. A gravity interpretation of the Benue Trough, Nigeria, *Tectonophysics*, 79, pp. 109–128.

Agagu, O.K. and Adighije, C.I, 1983. Tectonic and sedimentation framework of the lower Benue Trough, southeastern Nigeria, *Journal of African Earth Sciences (1983)*, 1(3–4), pp. 267–274. Available at: https://doi.org/10.1016/S0731-7247(83)80011-1.

Ajakaiye, D. E, Hall, D. H, Ashiekaa, J. A, Udensi, E. E, 1991. Magnetic anomalies in the Nigerian continental mass based on aeromagnetic surveys, *Tectonophysics*, 192(1–2), pp. 211–230. Available at: https://doi.org/10.1016/0040-1951(91)90258-T.

Ajakaiye, D.E. and Burke, K, 1973. A Bouguer gravity map of nigeria, *Tectonophysics*, 16(1–2). Available at: https://doi.org/10.1016/0040-1951(73)90134-0.

Ajayi, C.O, 1979. A Detailed Gravity Survey of the Middle Benue, Nigeria, *Unpublished Ph.D. thesis, Ahmadu Bello University* [Preprint].

Ajayi, C.O. and Ajakaiye, D.E, 1981. The Origin and Peculiarities of the Nigerian Benue Trough: Another look from Recent Gravity Data obtained from the Middle Benue, *Tectonophysics*, 80, pp. 285–303.

Ajayi, C.O. and Ajakaiye, D.E, 1986. Structures deduced from gravity data in the Middle Benue, Nigeria, *Journal of African Earth Sciences*, 5(4), pp. 359–369. Available at: https://doi.org/10.1016/0899-5362(86)90051-5.

Akande, S.O, Egenhoff, S.O, Obaje, N.G, Ojo, O.J, Adekeye, O.A, Erdtmann, B.D, 2012. Hydrocarbon potential of Cretaceous sediments in the Lower and Middle Benue Trough, Nigeria: Insights from new source rock facies evaluation, *Journal of African Earth Sciences*, 64, pp. 34–47. Available at: https://doi.org/10.1016/j.jafrearsci.2011.11.008.

Ali, M.Y, Fairhead, J.D, Green, C.M, 2017. Basement structure of the United Arab Emirates derived from an analysis of regional gravity and aeromagnetic database, *Tectonophysics*, 712–713, pp. 503–522. Available at: https://doi.org/10.1016/j.tecto.2017.06.006.

Anudu, G. K, Stephenson, R. A, Ofoegbu, C. O, Obrike, S. E, 2020. Basement morphology of the middle Benue Trough, Nigeria, revealed from analysis of high-resolution aeromagnetic data using grid-based operator methods, *Journal of African Earth Sciences*, 162(July 2019), p. 103724. Available at: https://doi.org/10.1016/j.jafrearsci.2019.103724.

Anudu, G.K., Stephenson, R.A. and Macdonald, D.I.M, 2014. Using high-resolution aeromagnetic data to recognise and map intra-sedimentary volcanic rocks and geological structures across the

754 Cretaceous middle Benue Trough, Nigeria, *Journal of African Earth Sciences*, 99, pp. 625–636.
755 Available at: https://doi.org/10.1016/j.jafrearsci.2014.02.017.

756 Arkani-Hamed, J., 1988. Differential reduction-to-the-pole of regional magnetic anomalies,
757 *Geophysics*, 53(12), pp. 1592–1600. Available at: https://doi.org/10.1190/1.1442441.

758 Arkani-Hamed, J, 2007. Differential reduction to the pole: Revisited, *Geophysics*, 72(1). Available at:
759 https://doi.org/10.1190/1.2399370.

760 Beard, L.P, 2000. Detection and identification of north-south trending magnetic structures near the
761 magnetic equator, *Geophysical Prospecting*, 48(4), pp. 745–761. Available at:
762 https://doi.org/10.1046/j.1365-2478.2000.00214.x.

763 Bello, R., Ofoha, C.C. and Wehiuzo, N, 2017. Re-evaluation of Sedimentary Thickness and Curie
764 Point Depth (CPD) of Parts of Lower Benue Trough and Anambra Basin , Nigeria , Using Regional
765 Magnetic Field Data, *Geosciences*, 7(3), pp. 95–107. Available at:
766 https://doi.org/10.5923/j.geo.20170703.02.

767 Benkhelil, J, 1989. The origin and evolution of the Cretaceous Benue Trough (Nigeria), *Journal of*
768 *African Earth Sciences*, 8(2–4), pp. 251–282. Available at: https://doi.org/10.1016/S0899-
769 5362(89)80028-4.

770 Binks, R.M. and Fairhead, J.D, 1992. A plate tectonic setting for Mesozoic rifts of West and Central
771 Africa, *Tectonophysics*, 213(1–2), pp. 141–151. Available at: https://doi.org/10.1016/0040-
772 1951(92)90255-5.

773 Bomfim, E.P., Braitenberg, C. and Molina, E.C, 2013. Mutual evaluation of global gravity models
774 (EGM2008 and GOCE) and terrestrial data in Amazon Basin, Brazil, *Geophysical Journal*
775 *International*, 195(2), pp. 870–882. Available at: https://doi.org/10.1093/gji/ggt283.

776 Cooper, G.R.J. and Cowan, D.R, 2005. Differential reduction to the pole, *67th European Association*
777 *of Geoscientists and Engineers, EAGE Conference and Exhibition, incorporating SPE EUROPE2005*
778 *- Extended Abstracts*, 67th Europ, pp. 1707–1710. Available at:
779 https://doi.org/10.1016/j.cageo.2005.02.005.

780 Coulon, C, Vidal, P, Dupuy, C, Baudin, P, Popoff, M, Maluski, H, Hermitte, D*,* 1996. The mesozoic
781 to early cenozoic magmatism of the Benue Trough (Nigeria); geochemical evidence for the
782 involvement of the St Helena Plume, *Journal of Petrology*, 37(6), pp. 1341–1358. Available at:
783 https://doi.org/10.1093/petrology/37.6.1341.

784 Cratchley, C.R. and Jones, G.P.G.P, 1965. An Interpretation of the Geology and Gravity Anomalies of
785 the Benue Valley, Nigeria, *Geophys. Pap. Overseas geol. Surv*, p. 413. Available at:
786 https://doi.org/10.2307/1793903.

787 Cratchley, C.R., Louis, P. and Ajakaiye, D.E, 1984. Geophysical and geological evidence for the
788 Benue- Chad Basin Cretaceous rift valley system and its tectonic implications, *Journal of African*
789 *Earth Sciences*, 2(2), pp. 141–150. Available at: https://doi.org/10.1016/s0731-7247(84)80008-7.

790 Cunningham, W.D. and Mann, P, 2007. *Tectonics of Strike-Slip Restraining and Releasing Bends.*
791 Geological Society, London, Special Publications 290, 143-168.

792 Deng, Y, Zhang, Z, Badal, J, Fan, W*,* 2014. 3-D density structure under South China constrained by
793 seismic velocity and gravity data. 627, pp. 159–170. Tectonophysics . Available at:
794 https://doi.org/10.1016/j.tecto.2013.07.032.

Fairhead, J.D, 1992. The West and Central African rift systems: Foreword. *Tectonophysics*, 213(1–2), pp. 139–140. Available at: https://doi.org/10.1016/0040-1951(92)90254-4.

Fairhead, J. D, Salem, A, Cascone, L, Hammill, M, Masterton, S, Samson, E, 2011. New developments of the magnetic tilt-depth method to improve structural mapping of sedimentary basins. *Geophysical Prospecting*, 59(6), pp. 1072–1086. Available at: https://doi.org/10.1111/j.1365-2478.2011.01001.x.

Fairhead, J.D, Green, C.M, Masterton, S.M, Guiraud, R, 2013. The role that plate tectonics, inferred stress changes and stratigraphic unconformities have on the evolution of the West and Central African Rift System and the Atlantic continental margins. *Tectonophysics*, 594, pp. 118–127. Available at: https://doi.org/10.1016/j.tecto.2013.03.021.

Fairhead, J.D, 2015. Advances in Gravity and Magnetic Processing and Interpretation. (EAGE Publications.). Available at: https://doi.org/10.3997/9789462821750.

Fairhead, J.D. and Binks, R.M, 1991. Differential opening of the Central and South Atlantic Oceans and the opening of the West African rift system, *Tectonophysics*, 187, pp. 191–203.

Fairhead, J.D. and Green, C.M, 1989. Controls on rifting in Africa and the regional tectonic model for the Nigeria and East Niger rift basins, *Journal of African Earth Sciences*, 8(2–4), pp. 231–249. Available at: https://doi.org/10.1016/S0899-5362(89)80027-2.

Fairhead, J.D. and Okereke, C.S, 1987. A regional gravity study of the West African rift system in Nigeria and Cameroon and its tectonic interpretation, *Tectonophysics*, 143(1–3), pp. 141–159. Available at: https://doi.org/10.1016/0040-1951(87)90084-9.

Fatoye, F.B. and Gideon, Y.B, 2013. Geology and mineral resources of the Northern Territory, 4(June), pp. 21–28.

Fedi, M. and Florio, G, 2001. Detection of potential fields source boundaries by enhanced horizontal derivative method, *Geophysical Prospecting*, 49(1), pp. 40–58. Available at: https://doi.org/10.1046/j.1365-2478.2001.00235.x.

Fitton, J.G,1980. The Benue trough and cameroon line - A migrating rift system in West Africa, *Earth and Planetary Science Letters*, 51(1), pp. 132–138. Available at: https://doi.org/10.1016/0012-821X(80)90261-7.

Foss, C, 2011. *Magnetic Data Enhancements and Depth Estimation*. In: Gupta H.K. (eds) Encyclopedia of Solid Earth Geophysics. Encyclopedia of Earth Sciences Series. Springer, Dordrecht. Available at: https://doi.org/10.1007/978-90-481-8702-7.

Geosoft, 2004. Topics in Gridding, *Technical Workshop* [Preprint].

Geosoft Inc, 2015. Defining and applying filters and inverse FFT in MAGMAP, *Www.Geosoft.Com*, pp. 1–27.

Ghazala, H.H, Ibraheem, I.M, Lamees, M, Haggag, M, 2018. Structural study using 2D modeling of the potential field data and GIS technique in Sohag Governorate and its surroundings, Upper Egypt, *NRIAG Journal of Astronomy and Geophysics*, 7(2), pp. 334–346. Available at: https://doi.org/10.1016/j.nrjag.2018.05.008.

Gómez-Ortiz, D. and Agarwal, B.N.P, 2005. 3DINVER.M: A MATLAB program to invert the gravity anomaly over a 3D horizontal density interface by Parker-Oldenburg's algorithm, *Computers and Geosciences*, 31(4), pp. 513–520. Available at: https://doi.org/10.1016/j.cageo.2004.11.004.

836 Guiraud, R. and Bosworth, W, 1997. Senonian basin inversion and rejuvenation of rifting in Africa
837 and Arabia: Synthesis and implications to plate-scale tectonics, *Tectonophysics*, 282(1–4), pp. 39–82.
838 Available at: https://doi.org/10.1016/S0040-1951(97)00212-6.

839 Guiraud, R. and Maurin, J.C, 1992. Early Cretaceous rifts of Western and Central Africa: an
840 overview, *Tectonophysics*, 213(1–2), pp. 153–168. Available at: https://doi.org/10.1016/0040-
841 1951(92)90256-6.

842 Habib, M. and Xie, C, 2012. Nigeria's inland basins : Investment opportunities and environment,
843 *Petroleum and Gas Exploration Research*, 2(11), pp. 202–211.

844 Hinze, W.J., Von Frese, R.R.B. and Saad, A.H, 2010. *Gravity and magnetic exploration: Principles,*
845 *practices, and applications*, *Gravity and Magnetic Exploration: Principles, Practices, and*
846 *Applications*. Available at: https://doi.org/10.1017/CBO9780511843129.

847 Hospers, J, 1965. Gravity Field of the Niger Delta (West Africa), *Nature*, (207), pp. 847–848.
848 Available at: https://doi.org/https://doi.org/10.1038/207847b0.

849 Hsieh, H.H, Chen, C.H, Lin, P.Y, Yen, H.Y, 2014. Curie point depth from spectral analysis of
850 magnetic data in Taiwan, *Journal of Asian Earth Sciences*, 90, pp. 26–33. Available at:
851 https://doi.org/10.1016/j.jseaes.2014.04.007.

852 Jiménez-Díaz, A, Ruiz, J, Pérez-Gussinyé, M, Kirby, J.F, Álvarez-Gómez, J.A, Tejero, R, Capote, R,
853 2014. Spatial variations of effective elastic thickness of the lithosphere in Central America and
854 surrounding regions, *Earth and Planetary Science Letters*, 391, pp. 55–66. Available at:
855 https://doi.org/10.1016/j.epsl.2014.01.042.

856 Li, X, 2008. Magnetic reduction-to-the-pole at low latitudes: Observations and considerations,
857 *Leading Edge (Tulsa, OK)*, 27(8), pp. 990–1002. Available at: https://doi.org/10.1190/1.2967550.

858 Li, Y. and Oldenburg, D.W, 1996. 3-D inversion of magnetic data, *Geophysics*, 61(3), pp. 394–408.
859 Available at: https://doi.org/10.1190/1.2711661.

860 Li, Y., Yang, Y. and Liu, T, 2010. Derivative-based techniques for geological contact mapping from
861 gravity data, *Journal of Earth Science*, 21(3), pp. 358–364. Available at:
862 https://doi.org/10.1007/s12583-010-0099-8.

863 Macleod, I. and Ellis, R, 2013. Magnetic Vector Inversion, a simple approach to the challenge of
864 varying direction of rock magnetization, *23rd International Geophysical Conference and Exhibition*,
865 (August), pp. 1–6. Available at: http://www.geosoft.com/media/uploads/resources/technical-
866 papers/aseg_2013_mvi_simple_approach_challenge_varying_direction_rock_magnetization.pdf.

867 MacLeod, I.N., Jones, K. and Dai, T.F, 1993. 3-D analytic signal in the interpretation of total
868 magnetic field data at low magnetic latitudes, *Exploration Geophysics*, 24(4), pp. 679–688. Available
869 at: https://doi.org/10.1071/EG993679.

870 MAG3D, 2017. A Program Library for Forward Modelling and Inversion of Magnetic Data over 3D
871 Structures, version 6. Available at: http://mag3d.readthedocs.io/en/v6/.

872 Mamah, L., Okogbue, C. and Onuoha, K., 2005. Inversion Tectonics of Benue Trough, pp. 163–167.

873 Mazur, S, Campbell, S, Green, C, Bouatmani, R, 2015. Extension across the Laptev Sea continental
874 rifts constrained by gravity modeling, *Tectonics*, 34(3), pp. 435–448. Available at:
875 https://doi.org/10.1002/2014TC003590.

McKenzie, D, 1978. Some remarks on the development of sedimentary basins, *Earth and Planetary Science Letters*, 40(1), pp. 25–32. Available at: https://doi.org/10.1016/0012-821X(78)90071-7.

Mickus, K. and Hussein, M, 2016. Curie Depth Analysis of the Salton Sea Region, Southern California, *Pure and Applied Geophysics*, 173(2), pp. 537–554. Available at: https://doi.org/10.1007/s00024-015-1100-3.

Najime, T, 2011. Depositional framework and Cretaceous stratigraphy of the Gboko Area Lower Benue Trough , Nigeria Introduction Cretaceous tectonic evolution and sedimentation along the Benue Trough was not uniform . This has led to the conventional sub-division of the tr, *Journal of Mining and Geology*, 47(2), pp. 147–165.

Nwachukwu, S.O, 1972. The tectonic evolution of the the southern portion of the Benue Trough, Nigeria, *Geological Magazine*, 109(5), pp. 411–419. Available at: https://doi.org/10.1017/S0016756800039790.

Nwankwo, L.I. and Sunday, A.J, 2017. Regional estimation of Curie-point depths and succeeding geothermal parameters from recently acquired high-resolution aeromagnetic data of the entire Bida Basin, north-central Nigeria, *Geothermal Energy Science*, 5(1), pp. 1–9. Available at: https://doi.org/10.5194/gtes-5-1-2017.

Obaje, N. G, Wehner, H, Scheeder, G, Abubakar, M. B, Jauro, A, 2004. Hydrocarbon prospectivity of Nigeria's inland basins: from the viewpoint of organic geochemistry and organic petrology, *American Association of Petroleum Geologists Bulletin*, Vol. 88(No. 3), pp. 325-353.

Obaje, N.G, Attah, D.O, Opeloye, S.A, Moumouni, A, 2006. Geochemical evaluation of the hydrocarbon prospects of sedimentary basins in Northern Nigeria, *Geochemical Journal*, 40(3), pp. 227–243. Available at: https://doi.org/10.2343/geochemj.40.227.

Obaje, N.G, 2009. *Geology and Mineral Resources of Nigeria*. Available at: https://doi.org/10.1007/978-3-540-92685-6.

Obasi, A.I., Selemo, A.O.I. and Nomeh, J.S, 2018. Gravity models as tool for basin boundary demarcation: A case study of Anambra Basin, Southeastern Nigeria, *Journal of Applied Geophysics*, 156, pp. 31–43. Available at: https://doi.org/10.1016/j.jappgeo.2017.11.002.

Ofoegbu, C.O, 1982. Methods of interpreting magnetic anomalies with application to the Minch dyke and magnetic anomalies over the lower and middle Benue trough of Nigeria, *Unpublished Ph.D. thesis, Durham University.* [Preprint].

Ofoegbu, C.O, 1985. A review of the geology of the Benue Trough, Nigeria, *Journal of African Earth Sciences*, 3(3), pp. 283–291. Available at: https://doi.org/10.1016/0899-5362(85)90001-6.

Oha, I.A, Onuoha, K.M, Nwegbu, A.N, Abba, A.U,, 2016. Interpretation of high resolution aeromagnetic data over southern benue trough, Southeastern Nigeria, *Journal of Earth System Science*, 125(2), pp. 369–385. Available at: https://doi.org/10.1007/s12040-016-0666-1.

Okereke, C.S, 1984. A gravity survey of the eastern sector of the Nigerian Basement Complex and studies of the gravity field of the West African Rift System, *Ph.D. Thesis, University of Leeds, Leeds (unpubl.).*, p. 272.

Okiwelu, A.A, Okwueze, E.E, Akpan, P.O, Ude, I.A, 2014. Basin Framework and Basement Structuring of Lower Benue Trough, West Africa based on Regional Magnetic Field Data: Tectonic and Hydrocarbon Implications, *Earth Science Research*, 4(1), pp. 1–20. Available at: https://doi.org/10.5539/esr.v4n1p1.

Olade, M.A, 1975. Evolution of Nigeria's Benue Trough (Aulacogen): A tectonic model, *Geological Magazine*, 112(6), pp. 575–583. Available at: https://doi.org/10.1017/S001675680003898X.

Oldenburg, D.W, 1994. The Inversion and Interpretation of Gravity Anomaly, 39(4), pp. 13–76.

Parker, R.L, 1972. The rapid calculation of potential anomalies, *Geophys. J. R. Astron. Soc.*, 31(4), pp. 447–455. Available at: papers://9e389b0a-9a01-4c38-a877-664a1ff838d5/Paper/p220.

Pham, L.T., Oksum, E. and Do, T.D, 2018. GCH_gravinv: A MATLAB-based program for inverting gravity anomalies over sedimentary basins, *Computers and Geosciences*, 120(February), pp. 40–47. Available at: https://doi.org/10.1016/j.cageo.2018.07.009.

Reford, S.W, Misener, D.J, Ugalde, H.A, Mcmaster, U, Gana, J.S, Oladele, O,, 2010. Nigeria's Nationwide High -resolution Airborne Geophysical Surveys Nigerias Nationwide High -resolution Airborne Geophysical Surveys, pp. 1835–1839.

Salem, A, Green, C, Fairhead, D, Aboud, E. 2012, 2012. Mapping basement relief of Abu Gharadig Basin, Western Desert of Egypt using 3D inversion of pseudo-gravity data, *ASEG Extended Abstracts*, 2012(1), pp. 1–4. Available at: https://doi.org/10.1071/aseg2012ab385.

Salem, A, Green, C, Cheyney, S, Fairhead, J.D, Aboud, E, Campbell, S, 2014. Mapping the depth to magnetic basement using inversion of pseudogravity: Application to the Bishop model and the Stord Basin, northern North Sea, *Interpretation*, 2(2), pp. 69–78. Available at: https://doi.org/doi:10.1190/INT-2013-0105.1.

Spector, A. and Grant, F.. S, 1970. Statistical models for interpreting aeromagnetic data, *Geophysics*, 35(2), pp. 293–302. Available at: https://doi.org/10.1190/1.1440092.

Speranza, F, Minelli, L, Pignatelli, A, Gilardi, M, 2016. Curie temperature depths in the Alps and the Po Plain (northern Italy): Comparison with heat flow and seismic tomography data, *Journal of Geodynamics*, 98, pp. 19–30. Available at: https://doi.org/10.1016/j.jog.2016.03.012.

Swain, C.J, 2000. Reduction-to-the-pole of regional magnetic data with variable field direction, and its stabilisation at low inclinations, *Exploration Geophysics*, 31(2), pp. 78–83. Available at: https://doi.org/10.1071/EG00078.

Tulyatid, J. and Fairhead, J.D, 1996. Application of combined aeromagnetic and radiometric mapping of geological structure in Central Thailand, *Paper presented at the 1996 SEG Annual Meeting, Denver, Colorado, November 1996*, pp. 1391–1394.

Vargas, R, Sainz-Maza Aparicio, S, Muñoz-Martín, A, Granja Bruña, J.L, Sentre Domingo, M.A, 2015. Gravity modeling of the lithosphere in the Calatrava Volcanic Province (Spain): geodynamic implications, *Journal of Iberian Geology*, 41(2), pp. 233–252. Available at: https://doi.org/10.5209/rev_jige.2015.v41.n2.47617.

Welford, J.K, Shannon, P.M, O'Reilly, B.M, Hall, J, 2010. Lithospheric density variations and Moho structure of the Irish Atlantic continental margin from constrained 3-D gravity inversion, *Geophysical Journal International*, 183(1), pp. 79–95. Available at: https://doi.org/10.1111/j.1365-246X.2010.04735.x.

Welford, J.K. and Hall, J, 2007. Crustal structure of the Newfoundland rifted continental margin from constrained 3-D gravity inversion, *Geophysical Journal International*, 171(2), pp. 890–908. Available at: https://doi.org/10.1111/j.1365-246X.2007.03549.x.

Wright, J, 1968. South Atlantic continental drift and the Benue Trough, *Tectonophysics*, 6(4), pp.

301–310. Available at: https://doi.org/10.1016/0040-1951(68)90046-2.

Yenne, E.Y, 2022. Integrating Gravity and Magnetic Data with Remote Sensing in Structural Modelling of Benue Trough (Middle and Lower) of Nigeria*, PhD thesis. University of Leeds*.